American Mineralogist, Volume 73, pages 809–817, 1988

High-temperature crystal structure of pyroxmangite

Linda R. Pinckney
Corning Glass Works, Sullivan Park FR-51, Corning, New York 14831, U.S.A.
Charles W. Burnham
Department of Earth and Planetary Sciences, Harvard University, Cambridge, Massachusetts 02138, U.S.A.

Abstract

High-temperature crystal-structure analysis of $MnSiO_3$ pyroxmangite indicates that expansion of the structure takes place by expansion of the M cation–containing polyhedra and of the void space between the polyhedra, with concomitant rotation of the relatively rigid tetrahedra about the bridging oxygens. Pyroxmangite displays a limited "inverse relationship" with respect to thermal expansion, compression, and chemical substitution, whereby structural changes resulting from the substitution of a larger cation for a smaller one are somewhat similar to those resulting from an increase in temperature or a decrease in pressure. The primary difference between the structural results of thermal expansion and chemical substitution is that increasing temperature causes long M–O bonds to expand faster than short bonds, whereas substituting larger cations into these sites causes shorter bonds to lengthen faster. All structural responses mirror those observed in pyroxenes.

Examination of the trends in structural parameters with temperature or compositional variation reveals no developing instabilities in the structure as observed limits are approached, which, coupled with thermodynamic information for these phases, indicates that there are no strong driving forces for phase transformations in the pyroxenoid system. Nevertheless, while no abrupt transformation to rhodonite takes place as temperature increases, a small amount of peak splitting is observed, suggesting incipient growth of rhodonite along (001) planes of the pyroxmangite. Such coherent growth has been confirmed by recent TEM studies of minerals in the pyroxene-pyroxenoid family.

Introduction

The pyroxenes and pyroxenoids are a closely related group of single-chain silicates that together constitute a polysomatic series. Each member is constructed of "layer modules" of the two end-member structures—wollastonite (W) and clinopyroxene (P). Although it has long been known that there are composition, temperature, and pressure limits to the stability fields of each of the members of the series, the influence of structure on these limits has not been examined until recently, particularly for low-Ca compositions.

In the preceding paper (Pinckney and Burnham, 1988), we have examined the structural changes in pyroxmangite (WPP) and rhodonite (WP) as a function of compositional variation in order to construct a rationale based on crystal structure to explain why one pyroxenoid phase is stabilized relative to another. Since the density of pyroxenoids increases with the number of P modules per unit cell (Akimoto and Syono, 1972), smaller cations, high pressure, and low temperature favor structures with large numbers of P modules.

The dependence of structure type on temperature is observed throughout the series of pyroxenes and pyroxenoids. The clinopyroxenes johannsenite ($CaMnSi_2O_6$; Morimoto et al., 1966), hedenbergite ($CaFeSi_2O_6$; Ruttstein, 1971), and possibly diopside ($CaMgSi_2O_6$; Pinckney and Burnham, 1981) transform to the bustamite structure at high temperatures and low pressures. Rhodonite also transforms to the bustamite structure (originally thought to be the wollastonite structure) as temperature increases (Dent Glasser and Glasser, 1961).

Compositions close to $MnSiO_3$ exist naturally in both the pyroxmangite and rhodonite structures, and the pure phase has been synthesized with the clinopyroxene and garnet structures at high pressure (Akimoto and Syono, 1972). The pyroxmangite-rhodonite transformation for this composition has been studied by several workers, among them Momoi (1974) and Maresch and Mottana (1976). Pyroxmangite is the high-pressure, low-temperature polymorph with respect to rhodonite. The exact location of the equilibrium curve, however, is unknown; in fact, the determination of the stable phase at ambient conditions remains in question.

It is useful to be able to correlate such phase transitions with actual changes in the crystal structure as temperature or pressure increases. Nevertheless, there exists no information on the high-temperature or high-pressure crystal structures of these phases. An in situ, high-temperature study of the crystal structure of pyroxmangite therefore has been carried out in order to examine in detail the

0003–004X/88/0708–0809$02.00

structure expansion, to search for any developing structural mismatches, to investigate possible mechanisms for a pyroxmangite-rhodonite inversion, and possibly to observe this transformation. Preliminary results from this study were reported by Pinckney et al. (1981).

Experimental methods

The pyroxmangite samples used in this study are from a metamorphosed manganese ore deposit at the Ajiro mine, Honshu, Japan, and were supplied by Gordon E. Brown, Jr., of Stanford University. Electron-microprobe analyses of a number of separated crystals yield a composition of $(Mn_{0.97}Mg_{0.02}Ca_{0.01})SiO_3$, with no observed inhomogeneities or inclusions.

High temperature

A clear crystal 0.17 × 0.12 × 0.085 mm was mounted in an evacuated silica-glass capillary. Intensity measurements were carried out with Nb-filtered Mo$K\alpha$ radiation on the automated four-circle diffractometer at the Geophysical Laboratory of the Carnegie Institution of Washington (Finger et al., 1973). A radiative-type heater was employed, consisting of a Pt-resistance heating assembly mounted directly onto the χ-circle of the diffractometer. A sensing thermocouple near the crystal was used as input to a computer-operated controller.

Intensity data were collected at 24, 200, 400, and 600 °C. The crystal was allowed to equilibrate at each temperature for at least 1 h before any measurements were made. Cell parameters were measured at 100 °C intervals as well as before and after measurement of each data set. Data collection was underway at 800 °C when the furnace leads short-circuited; data collection was then terminated.

Corrections were made for Lorentz and polarization effects and for crystal absorption ($\mu_l = 36.5$ cm^{-1}). Diffractions having an intensity less than $2\sigma_I$ were rejected from the subsequent structural analysis. Least-squares refinement was initiated with the computer program RFINE (Finger and Prince, 1975), using the atomic coordinates and site occupancies determined in a previous room-temperature refinement of another crystal of the same material that yielded results essentially equal to those reported herein. These site occupancies are recorded in Pinckney and Burnham (1988) and were not varied in these refinements. Atomic scattering factors for Mn^{2+}, Mg^{2+}, Si^{4+}, and O^{2-} and anomalous dispersion corrections were taken from Cromer and Mann (1968) and Cromer (1965), respectively.

The results of this refinement are listed in Table 1. The final weighted residuals, R_w, ranged from 4.3 to 5.5%. An average of seven cycles of least-squares refinement were completed for each temperature. All diffractions were weighted by $1/\sigma_F^2$, where σ_F is the estimated standard deviation of the observation based on counting statistics (Burnham et al., 1971).

Final atomic positional parameters and equivalent isotropic temperature factors for pyroxmangite at 24, 200, 400, and 600 °C are given in Tables 2 and 3. Selected interatomic distances and polyhedral volumes and distortions are listed in Tables 4 and 5. In the absence of a good model describing the effect of thermal vibration on these bond distances, the Si–O distances are not corrected for thermal motion and therefore appear to shorten slightly as temperature increases. For the M–O distances, a correction for noncorrelated motion, intermediate between correlated parallel and antiparallel motion, was computed by the least-squares refinement program RFINE using equations cited by Busing and Levy (1964). Mean M–O bond distances have been calculated using the individually corrected M–O distances and are included in Table 4.

TABLE 1. Data collection and refinement conditions for pyroxmangite

	24 °C	200 °C	400 °C	600 °C
sin θ/λ max	0.65	0.60	0.60	0.60
Number of measurements	3760	2867	2900	2900
Number observed ($I > 2\sigma$)	2609	1969	1960	1818
Weighted R	0.047	0.055	0.043	0.046
Unweighted R	0.054	0.069	0.057	0.066

High pressure

The cell parameters of pyroxmangite were also measured at 20 kbar, although no structure refinement was carried out. A small crystal of pyroxmangite was mounted in a diamond-anvil X-ray cell (Merrill and Bassett, 1974) as modified by Hazen and Finger (1977). A ruby chip was included in the mount for pressure calibration, and a 4:1 mixture of methanol : ethanol was employed as the hydrostatic pressure medium. Pressure calibration before and after cell-parameter measurements indicated that the pressure remained constant throughout the data collection.

Results

The structure of pyroxmangite has been described elsewhere (e.g., Ohashi and Finger, 1975). We employ the C-centered unit cell ($C\bar{1}$, Z = 28), with the tetrahedral chain parallel to the c axis and nearly closest-packed oxygen layers parallel to (100).

Cell-parameter data are listed in Table 6. Axial lengths a, b, and c increase linearly with temperature. Figure 1 illustrates the variation of cell parameters with normalized unit-cell volume V/V_0, where V_0 is the cell volume at room temperature and pressure. This plot incorporates all the high-temperature data as well as the measurement taken at 20 kbar. Despite the complexity of the pyroxmangite structure, the high-pressure cell edges and the angle γ fall on the plot defined by the high-temperature data, which indicates that pyroxmangite displays an "inverse relationship" between thermal expansion and bulk compression of the kind described by Hazen and Prewitt (1977). This is because the only cation–oxygen bonds in this structure to exhibit significant expansion or compression are the Mn–O bonds; the Si–O bond lengths change very little with temperature and, by analogy with pyroxenes (e.g., Levien and Prewitt, 1981), very little with pressure.

The linear thermal expansion and bulk compression coefficients of the cell edges are given in Table 7. The relative expansions of the edges, $b > a > c$, as well as their relative compressions, $b > c > a$, are the same as that of $C2/c$ pyroxenes and reflect the basic correspondence of the pyroxmangite and pyroxene structures.

The magnitudes and orientations of the unit-cell strain ellipsoids for thermal expansion and bulk compression are given in Table 8. Although an increase in temperature and the substitution of larger cations for smaller have the same general effects on a structure (the cell volume expands, the tetrahedral chain straightens, and so on), the

TABLE 2. Ajiro pryoxmangite atom coordinates at several temperatures

	24 °C			200 °C			400 °C		
	x	*y*	*z*	*x*	*y*	*z*	*x*	*y*	*z*
M1	−0.0014(2)	0.0415(2)	0.1050(1)	−0.0014(3)	0.0411(3)	0.1052(2)	−0.0013(2)	0.0401(2)	0.1052(1)
M2	−0.0017(2)	0.1695(2)	0.3124(1)	−0.0015(3)	1.1695(3)	0.3129(2)	−0.0018(2)	0.1693(2)	0.3132(1)
M3	0.0016(2)	0.0686(2)	0.6057(1)	0.0022(3)	0.0694(3)	0.6059(2)	0.0021(2)	0.0709(2)	0.6063(1)
M4	0.0144(2)	0.1766(2)	0.8064(1)	0.0154(3)	0.1776(3)	0.8067(2)	0.0159(2)	0.1782(2)	0.8069(1)
M5	0.0040(2)	0.2698(2)	0.5098(1)	0.0040(3)	0.2698(3)	0.5099(2)	0.0042(2)	0.2695(2)	0.5095(1)
M6	0.0618(2)	0.2634(2)	0.0177(1)	0.0628(3)	0.2642(3)	0.0186(2)	0.0626(3)	0.2647(2)	0.0190(1)
M7	−0.0089(2)	0.3693(2)	0.2087(1)	−0.0097(3)	0.3696(3)	0.2094(2)	−0.0103(2)	0.3687(2)	0.2095(1)
Si1	0.2024(4)	0.4433(4)	0.9350(2)	0.2034(5)	0.4438(5)	0.9354(4)	0.2037(4)	0.4438(3)	0.9360(2)
Si2	0.2109(4)	0.3322(4)	0.7517(2)	0.2117(6)	0.3334(6)	0.7524(4)	0.2119(4)	0.3338(3)	0.7522(2)
Si3	0.2124(4)	0.5318(4)	0.6627(2)	0.2126(6)	0.5328(6)	0.6629(4)	0.2129(4)	0.5327(4)	0.6625(2)
Si4	0.2071(4)	0.4258(4)	0.4697(2)	0.2069(6)	0.4261(6)	0.4701(4)	0.2073(4)	0.4252(4)	0.4696(2)
Si5	0.2096(4)	0.6318(4)	0.3805(2)	0.2108(6)	0.6308(6)	0.3805(4)	0.2099(4)	0.6307(4)	0.3801(2)
Si6	0.2080(4)	0.5296(4)	0.1895(2)	0.2077(6)	0.5289(6)	0.1901(4)	0.2072(4)	0.5289(4)	0.1897(2)
Si7	0.2036(4)	0.7101(4)	0.0895(2)	0.2036(6)	0.7091(6)	0.0895(4)	0.2035(4)	0.7088(3)	0.0895(2)
OA1	0.1298(9)	0.0709(9)	0.0288(6)	0.1298(14)	0.0723(14)	0.0302(9)	0.1308(9)	0.0716(8)	0.0299(5)
OA2	0.1194(9)	0.1877(9)	0.2267(6)	0.1198(14)	0.1877(14)	0.2276(9)	0.1198(9)	0.1863(8)	0.2272(5)
OA3	0.1186(9)	0.9632(9)	0.3105(6)	0.1194(13)	0.9634(13)	0.3111(8)	0.1191(9)	0.9620(9)	0.3112(5)
OA4	0.1232(9)	0.0908(9)	0.5206(6)	0.1254(14)	0.0925(14)	0.5214(9)	0.1250(9)	0.0914(9)	0.5212(5)
OA5	0.1208(9)	0.8706(9)	0.6051(6)	0.1218(14)	0.8727(14)	0.6063(9)	0.1225(9)	0.8719(9)	0.6052(5)
OA6	0.1246(9)	0.9864(9)	0.8061(6)	0.1266(13)	0.9888(13)	0.8072(8)	0.1265(9)	0.9887(9)	0.8073(5)
OA7	0.1308(9)	0.7794(9)	0.8969(6)	0.1318(14)	0.7827(13)	0.8981(9)	0.1336(9)	0.7804(8)	0.8958(5)
OA8	0.0984(9)	0.8418(9)	0.0943(6)	0.0091(12)	0.8406(12)	0.0945(8)	0.0991(8)	0.8394(8)	0.0940(5)
OB1	0.1300(9)	0.3123(9)	0.9293(6)	0.1322(14)	0.3096(14)	0.9288(9)	0.1320(8)	0.3135(8)	0.9316(5)
OB2	0.1255(9)	0.1977(9)	0.7239(6)	0.1258(14)	0.1968(14)	0.7222(9)	0.1255(9)	0.2009(8)	0.7236(5)
OB3	0.1236(9)	0.6625(9)	0.7132(6)	0.1248(14)	0.6603(14)	0.7107(9)	0.1238(9)	0.6634(8)	0.7114(5)
OB4	0.1220(9)	0.2883(9)	0.4275(6)	0.1215(14)	0.2907(14)	0.4267(9)	0.1218(9)	0.2898(8)	0.4281(5)
OB5	0.1284(9)	0.7745(9)	0.4216(6)	0.1293(14)	0.7709(14)	0.4217(9)	0.1274(9)	0.7718(8)	0.4212(5)
OB6	0.1210(9)	0.3967(9)	0.1340(6)	0.1225(14)	0.3974(14)	0.1341(9)	0.1214(9)	0.3969(9)	0.1357(6)
OC1	0.1666(8)	0.4496(8)	0.8403(5)	0.1699(13)	0.4474(13)	0.8388(8)	0.1706(8)	0.4487(8)	0.8410(5)
OC2	0.1625(8)	0.4013(8)	0.6791(5)	0.1640(12)	0.4025(12)	0.6816(8)	0.1642(8)	0.4046(8)	0.6809(5)
OC3	0.1610(9)	0.4997(9)	0.5619(6)	0.1626(13)	0.5001(12)	0.5637(8)	0.1630(8)	0.4977(8)	0.5616(5)
OC4	0.1518(9)	0.5315(9)	0.4190(6)	0.1531(13)	0.5313(12)	0.4184(8)	0.1533(8)	0.5301(8)	0.4191(5)
OC5	0.1544(9)	0.5677(9)	0.2780(6)	0.1550(13)	0.5672(12)	0.2783(8)	0.1557(9)	0.5676(9)	0.2790(6)
OC6	0.1569(9)	0.6595(9)	0.1581(6)	0.1562(13)	0.6617(12)	0.1610(8)	0.1568(8)	0.6570(8)	0.1581(5)
OC7	0.1431(9)	0.5919(9)	0.9975(6)	0.1459(13)	0.5920(12)	0.9965(8)	0.1454(8)	0.5912(8)	0.9976(5)

detailed effects can be quite different. For example, the orientation of the strain ellipsoid caused by thermal expansion resembles only vaguely that caused by the addition of larger cations to pyroxmangite (Pinckney and Burnham, 1988). The difference in orientation is due to the dissimilar nature of Mn–O bond expansion caused by temperature and by cation substitution: as the occupancy of a large cation in a polyhedron increases, short M–O bonds expand more than long bonds, whereas with increasing temperature, long bonds generally expand faster than short ones. This effect has also been observed in pyroxenes by Ohashi and Burnham (1973).

Overall, the directions of maximum and minimum thermal expansion are quite similar to those exhibited by diopside (Finger and Ohashi, 1976). The smallest amount of expansion (ϵ_3) is only approximately along *c*, the chain direction; it appears that the response of the metal–oxygen bonds plays at least as important a role in the structure expansion as does the "rigid" behavior of the silicate chains.

Silicate chain

The tetrahedral chain responds in essentially the same way to expansion of the octahedral bands regardless of whether that expansion is due to increased temperature or to the substitution of larger cations. Individual tetrahedra remain essentially the same size over this temperature range, although their distortion decreases slightly, and there are no significant changes in Si-Si distances. The tetrahedral chain angles "straighten" by up to 3°, although the average change is less than 1° (Table 9). It is interesting, however, to note that several of the chain angles, notably OC1-OC2-OC3, OC7-OC1-OC2, and to a lesser extent OC6-OC7-OC1, adjust so as to approach more closely their rhodonite equivalents OC1-OC2-OC3 (154.6°), OC5-OC1-OC2 (154.1°), and OC4-OC5-OC1 (160.0°), respectively, as determined by Narita et al. (1977).

Octahedral band

All Mn–O bonds expand more than Si–O bonds, and generally long Mn–O bonds expand faster than short ones. The mean thermal expansion coefficients for mean M–O distances and polyhedral volumes for the temperature range 24–600 °C are listed in Table 10. The M3 and M4 cation polyhedra undergo the most expansion over this temperature range, while the M1 octahedron expands the least; M1 is the site most constrained by surrounding cations and by the silicate chain stretched across it. The distortion parameters of the inner octahedra (Table 5),

TABLE 2—*Continued*

600 °C		
x	*y*	*z*
−0.0015(3)	0.0391(3)	0.1050(2)
−0.0016(3)	0.1693(3)	0.3135(2)
0.0020(3)	0.0720(3)	0.6064(2)
0.0164(3)	0.1792(3)	0.0872(2)
0.0042(3)	0.2694(3)	0.5094(2)
0.0631(3)	0.2654(3)	0.0197(2)
−0.0108(3)	0.3686(3)	0.2101(2)
0.0247(4)	0.4438(4)	0.9362(3)
0.2124(5)	0.3353(4)	0.7527(3)
0.2139(5)	0.5337(5)	0.6628(3)
0.2072(5)	0.4252(5)	0.4692(3)
0.2104(5)	0.6300(5)	0.3803(3)
0.2071(5)	0.5281(5)	0.1898(3)
0.2027(4)	0.7083(4)	0.0895(3)
0.1304(10)	0.0720(10)	0.0301(6)
0.1198(10)	0.1856(10)	0.2279(6)
0.1198(10)	0.9623(10)	0.3125(6)
0.1268(11)	0.0927(11)	0.5221(7)
0.1235(11)	0.8720(11)	0.6052(7)
0.1268(10)	0.9897(10)	0.8076(6)
0.1331(10)	0.7811(10)	0.8952(6)
0.0981(10)	0.8377(10)	0.0941(6)
0.1327(10)	0.3150(10)	0.9326(7)
0.1258(10)	0.2025(10)	0.7241(7)
0.1245(10)	0.6630(10)	0.7115(7)
0.1213(11)	0.2903(11)	0.4281(7)
0.1275(11)	0.7698(11)	0.4209(7)
0.1198(10)	0.3967(10)	0.1365(7)
0.1714(9)	0.4486(9)	0.8419(6)
0.1649(10)	0.4060(10)	0.6822(6)
0.1646(10)	0.4962(10)	0.5611(7)
0.1546(5)	0.5300(10)	0.4193(6)
0.1564(10)	0.5677(10)	0.2793(6)
0.1570(10)	0.6574(10)	0.1581(6)
0.1469(10)	0.5913(10)	0.9977(6)

TABLE 3. Equivalent isotropic temperature factors of pyroxmangite at four temperatures (Å²)

	24 °C	200 °C	400 °C	600 °C
M1	0.6(1)	1.2(2)	1.5(1)	2.0(1)
M2	0.6(1)	1.1(2)	1.5(1)	2.0(1)
M3	0.6(1)	1.0(2)	1.4(1)	1.9(1)
M4	0.6(1)	1.1(2)	1.6(1)	2.1(1)
M5	0.9(1)	1.5(2)	2.0(1)	2.7(1)
M6	0.9(1)	1.7(2)	2.2(1)	2.8(1)
M7	0.9(1)	1.5(2)	2.1(1)	2.8(1)
Si1	0.6(1)	0.9(2)	1.2(2)	1.4(2)
Si2	0.5(1)	0.8(3)	1.0(2)	1.3(2)
Si3	0.5(1)	0.9(3)	1.1(2)	1.4(2)
Si4	0.5(1)	0.7(3)	1.1(2)	1.4(2)
Si5	0.5(1)	0.8(3)	1.0(2)	1.3(2)
Si6	0.5(1)	0.7(3)	1.1(2)	1.2(2)
Si7	0.5(1)	0.7(2)	1.1(2)	1.2(2)
OA1	0.7(4)	1.3(7)	1.5(4)	1.8(6)
OA2	0.6(4)	1.0(7)	1.2(4)	1.3(5)
OA3	0.7(4)	0.7(7)	1.3(4)	1.6(6)
OA4	0.6(4)	1.2(7)	1.5(5)	2.1(6)
OA5	0.6(4)	0.7(7)	1.4(4)	1.7(6)
OA6	0.6(4)	1.1(7)	1.5(4)	1.8(6)
OA7	0.6(4)	1.1(7)	1.3(5)	1.6(6)
OA8	0.6(3)	1.0(6)	1.4(4)	1.8(5)
OB1	0.8(4)	1.6(8)	1.6(4)	2.1(6)
OB2	0.8(4)	1.1(7)	1.4(5)	1.8(6)
OB3	0.6(4)	1.1(7)	1.5(5)	2.0(6)
OB4	0.7(4)	1.2(7)	1.6(5)	2.2(6)
OB5	0.7(4)	1.1(7)	1.6(5)	2.1(6)
OB6	0.7(4)	0.8(7)	1.6(5)	1.8(6)
OC1	0.6(3)	1.3(6)	1.3(4)	1.7(5)
OC2	0.6(3)	1.2(6)	1.6(4)	2.1(6)
OC3	0.7(3)	1.3(7)	1.7(4)	2.3(6)
OC4	0.8(4)	1.2(6)	1.8(5)	2.2(6)
OC5	0.8(3)	1.0(6)	2.0(5)	2.4(6)
OC6	0.6(3)	0.9(6)	1.4(4)	1.8(6)
OC7	0.6(3)	1.3(7)	1.4(5)	1.9(6)

with six regular M–O bonds, remain essentially constant over this temperature range. The M2 octahedron shows no signs of taking on the rhodonite-like characteristics described by Pinckney and Burnham (1988), wherein the rhodonite M2 octahedron is observed to be consistently larger and more distorted than the equivalent M2 octahedron in pyroxmangite of the same composition.

Thermal parameters

As temperature increases, equivalent isotropic temperature factors (Table 3) increase at the lowest rate for Si atoms and, not unexpectedly, at the highest rate for the irregularly coordinated M5, M6, and M7 cations. The ellipsoids for both the M and Si cations possess their longest *rms* displacements approximately perpendicular to the *b* axis, and the bridging oxygens have their longest axes perpendicular to their associated Si–O bonds, that is, perpendicular to *c* as well as to *b*.

DISCUSSION

Comparison of chemical substitution and temperature effects

Increasing temperature has a less pronounced effect on the pyroxmangite structure than does cation substitution over the observed range; nonetheless, a number of structural parameters show strikingly similar responses to these variables. The relative cell-edge expansion for both increased temperature and the substitution of a larger cation is identical: $b > a > c$. The variation of cell edges with normalized unit-cell volume is plotted in Figure 2 for pyroxmangites of various compositions as well as for the Ajiro pyroxmangite at high temperatures and pressure. The linearity of the composite plots is quite remarkable considering the wide composition range and the different orientations of the strain ellipsoid caused by increasing temperature and by substituting a larger cation.

Another striking parallel between temperature and compositional variation lies in the correlation between the average sizes of the M1*i* cation octahedra on the inside of the octahedral band and those of the outer M2*j* polyhedra (Pinckney and Burnham, 1988). Figure 3 is a plot of the average bond lengths of the M2*j* polyhedra as a function of those of their corresponding M1*i* octahedra for pyroxmangites and rhodonites of various compositions, including Ca-rich pyroxferroite, as well as for pyroxmangite at high temperature. The coincidence of these curves confirms that the M1*i* octahedra do indeed constrain the ultimate size of the M2*j* polyhedra and may

TABLE 4. Selected interatomic distances for Ajiro pyroxmangite (Å)

	24 °C	200 °C	400 °C	600 °C		24 °C	200 °C	400 °C	600 °C
M1–OA1	2.1558(3)	2.147(2)	2.161(2)	2.160(2)	M7–OA2	2.2374(5)	2.246(2)	2.250(1)	2.258(1)
–OA1	2.3211(5)	2.341(3)	2.339(3)	2.335(3)	–OA7	2.1344(5)	2.169(3)	2.141(2)	2.139(2)
–OA2	2.2628(5)	2.274(3)	2.267(2)	2.278(2)	–OB3	2.0789(3)	2.098(2)	2.085(2)	2.075(2)
–OA6	2.2757(3)	2.280(2)	2.273(2)	2.272(2)	–OB6	2.1162(3)	2.142(2)	2.120(2)	2.109(2)
–OA7	2.1422(5)	2.127(2)	2.155(1)	2.152(1)	–OC1	2.5809(5)	2.597(2)	2.615(1)	2.630(2)
–OA8	2.1639(5)	2.174(2)	2.174(1)	2.179(1)	–OC5	2.5293(6)	2.533(2)	2.550(2)	2.558(2)
Mean	2.2203(5)	2.224(2)	2.228(2)	2.229(2)	–OC2	2.9574(7)	2.927(3)	2.922(2)	2.903(3)
(Corr.)		2.236	2.246	2.250	Mean(7)	2.3764(5)	2.387(2)	2.383(2)	2.382(2)
					(Corr.)		2.401	2.403	2.407
M2–OA2	2.1702(3)	2.165(2)	2.172(2)	2.164(2)	Mean(6)	2.2795(5)	2.297(2)	2.293(2)	2.295(2)
–OA6	2.2831(6)	2.318(3)	2.318(2)	2.331(3)	(Corr.)		2.312	2.314	2.321
–OA3	2.3297(5)	2.332(2)	2.341(1)	2.345(2)					
–OA5	2.2156(3)	2.221(2)	2.217(2)	2.223(2)					
–OB3	2.1402(5)	2.152(2)	2.128(1)	2.137(1)	Si1–OA1	1.6210(4)	1.609(2)	1.595(1)	1.590(1)
–OB4	2.1071(5)	2.099(3)	2.110(2)	2.105(3)	–OB1	1.5850(3)	1.603(1)	1.582(1)	1.576(1)
Mean	2.2077(5)	2.213(2)	2.214(2)	2.217(2)	–OC1	1.6370(3)	1.658(2)	1.635(2)	1.622(2)
(Corr.)		2.225	2.232	2.239	–OC7	1.6547(4)	1.638(1)	1.639(1)	1.636(1)
					Mean	1.6244(3)	1.627(2)	1.613(1)	1.606(1)
M3–OA3	2.1988(3)	2.202(2)	2.194(2)	2.183(2)					
–OA4	2.1822(3)	2.187(2)	2.183(2)	2.186(2)	Si2–OA2	1.6128(4)	1.602(2)	1.599(1)	1.594(1)
–OA4	2.3801(6)	2.410(3)	2.412(2)	2.439(3)	–OB2	1.5889(4)	1.603(1)	1.579(1)	1.577(1)
–OA5	2.2552(5)	2.250(2)	2.267(1)	2.280(1)	–OC2	1.6430(3)	1.615(2)	1.635(1)	1.622(1)
–OB2	2.1733(5)	2.147(3)	2.167(2)	2.174(3)	–OC1	1.6772(3)	1.633(2)	1.664(2)	1.662(2)
–OB5	2.0894(5)	2.122(2)	2.093(1)	2.098(1)	Mean	1.6304(3)	1.613(2)	1.619(1)	1.614(1)
Mean	2.2132(5)	2.220(2)	2.219(2)	2.227(2)					
(Corr.)		2.233	2.236	2.249	Si3–OA3	1.6049(4)	1.594(2)	1.595(1)	1.578(1)
					–OB3	1.5959(4)	1.555(1)	1.588(1)	1.580(1)
M4–OA3	2.2417(5)	2.263(3)	2.263(2)	2.289(3)	–OC3	1.6296(3)	1.602(2)	1.624(2)	1.634(2)
–OA6	2.1512(5)	2.146(2)	2.150(1)	2.149(1)	–OC2	1.6512(3)	1.667(1)	1.643(1)	1.650(1)
–OA8	2.3218(4)	2.322(2)	2.329(2)	2.316(2)	Mean	1.6204(3)	1.604(2)	1.613(1)	1.611(1)
–OB1	2.2162(5)	2.198(3)	2.235(2)	2.245(3)					
–OB2	2.0669(3)	2.086(2)	2.076(2)	2.076(2)	Si4–OA4	1.6134(4)	1.597(2)	1.595(1)	1.580(1)
–OC6	2.2550(6)	2.229(2)	2.267(1)	2.264(2)	–OB4	1.5941(4)	1.579(1)	1.579(1)	1.577(1)
Mean	2.2088(5)	2.207(2)	2.220(2)	2.223(2)	–OC4	1.6426(3)	1.648(1)	1.631(1)	1.620(1)
(Corr.)		2.218	2.237	2.246	–OC3	1.6380(3)	1.652(2)	1.628(2)	1.617(2)
					Mean	1.6220(3)	1.619(2)	1.608(1)	1.599(1)
M5–OA5	2.1893(5)	2.214(3)	2.200(2)	2.204(3)					
–OA4	2.1366(5)	2.135(2)	2.139(1)	2.140(1)	Si5–OA5	1.6084(4)	1.588(2)	1.590(1)	1.574(1)
–OB4	2.1044(3)	2.120(2)	2.093(2)	2.090(2)	–OB5	1.5951(4)	1.578(1)	1.589(1)	1.580(1)
–OB5	2.1343(3)	2.120(2)	2.121(1)	2.118(2)	–OC5	1.6396(3)	1.635(2)	1.617(2)	1.615(2)
–OC3	2.7652(7)	2.774(2)	2.760(1)	2.759(2)	–OC4	1.6524(3)	1.638(1)	1.654(1)	1.648(1)
–OC4	2.5134(6)	2.525(2)	2.533(2)	2.542(2)	Mean	1.6239(3)	1.610(2)	1.612(1)	1.604(1)
–OC2	2.9014(6)	2.940(4)	2.938(3)	2.960(4)					
Mean(7)	2.3915(5)	2.404(3)	2.398(2)	2.402(2)	Si6–OA6	1.6020(4)	1.589(2)	1.594(1)	1.593(1)
(Corr.)		2.417	2.417	2.427	–OB6	1.5854(4)	1.568(2)	1.569(1)	1.570(1)
Mean(6)	2.3065(5)	2.315(2)	2.308(2)	2.309(2)	–OC6	1.6420(3)	1.648(1)	1.628(1)	1.638(1)
(Corr.)		2.328	2.328	2.336	–OC5	1.6292(3)	1.621(2)	1.632(2)	1.629(2)
					Mean	1.6147(3)	1.607(2)	1.606(1)	1.608(1)
M6–OA1	2.1209(5)	2.116(1)	2.126(1)	2.123(1)					
–OA8	2.2135(5)	2.232(3)	2.228(2)	2.231(3)	Si7–OA7	1.5845(4)	1.573(2)	1.557(1)	1.567(1)
–OB1	2.0526(3)	2.062(2)	2.043(2)	2.044(2)	–OA8	1.6065(4)	1.601(1)	1.594(1)	1.585(1)
–OB6	1.9872(4)	1.978(2)	1.988(2)	1.981(2)	–OC7	1.6503(4)	1.650(2)	1.641(2)	1.633(2)
–OC7	2.3840(6)	2.404(2)	2.404(1)	2.418(2)	–OC6	1.6429(2)	1.672(2)	1.652(1)	1.641(1)
–OA7	2.8067(5)	2.815(3)	2.845(2)	2.848(2)	Mean	1.6211(3)	1.624(2)	1.611(1)	1.606(1)
Mean(6)	2.2608(5)	2.268(2)	2.272(2)	2.274(2)					
(Corr.)		2.285	2.294	2.302					
Mean(5)	2.1516(5)	2.159(2)	2.158(2)	2.160(2)					
(Corr.)		2.177	2.181	2.190					

aptly be considered the major building blocks of the pyroxene-pyroxenoid structures.

Close examination of the changes produced in the pyroxmangite and rhodonite structures by chemical substitution and in pyroxmangite by increasing temperature, while revealing several minor structural mismatches, yields no significant evidence of developing structural instabilities that might limit the stability fields of these minerals. Cell parameters, polyhedral volumes and distortions, and individual bond lengths and angles all change smoothly with temperature. There is no greatly increased misfit between the octahedral bands and tetrahedral chains, for example, analogous to the misfit between octahedral and tetrahedral sheets that is thought to lead to stability limits in the micas (Hazen and Wones, 1978). There appears, therefore, to be no strong driving force of structural origin toward a pyroxmangite-rhodonite phase transformation, which may explain the experimental problems in achieving equilibrium and the widespread persistence of metastable phases observed in both experimental and natural environments (e.g., Abrecht and Peters, 1980; Aikawa, 1984).

TABLE 5. Ajiro pyroxmangite: Tetrahedral and octahedral volumes and distortions

		24 °C	200 °C	400 °C	600 °C
			Tetrahedral		
Si1	V	2.19	2.20	2.17	2.16
	λ	1.0040	1.0049	1.0034	1.0032
	σ^2	14.50	18.55	12.20	11.66
Si2	V	2.22	2.15	2.17	2.19
	λ	1.0037	1.0034	1.0039	1.0035
	σ^2	15.49	14.28	16.72	15.06
Si3	V	2.17	2.11	2.16	2.17
	λ	1.0040	1.0049	1.0040	1.0049
	σ^2	17.09	19.84	17.60	21.32
Si4	V	2.17	2.17	2.14	2.12
	λ	1.0054	1.0042	1.0055	1.0054
	σ^2	22.66	17.54	23.28	22.74
Si5	V	2.18	2.12	2.15	2.13
	λ	1.0079	1.0096	1.0082	1.0081
	σ^2	33.51	40.84	34.95	34.54
Si6	V	2.12	2.09	2.11	2.13
	λ	1.0122	1.0117	1.0114	1.0120
	σ^2	49.66	46.25	45.91	48.56
Si7	V	2.15	2.16	2.14	2.13
	λ	1.0121	1.0123	1.0110	1.0111
	σ^2	54.88	54.39	50.01	49.99
			Octahedral		
M1	V	14.21	14.30	14.53	14.64
	λ	1.020	1.020	1.019	1.020
	σ^2	60.88	58.84	59.09	59.98
M2	V	14.03	14.16	14.33	14.49
	λ	1.016	1.016	1.016	1.016
	σ^2	53.53	48.16	51.31	50.10
M3	V	14.14	14.35	14.47	14.73
	λ	1.015	1.014	1.015	1.015
	σ^2	45.58	40.44	43.14	40.28
M4	V	13.41	13.44	13.78	13.90
	λ	1.049	1.046	1.048	1.049
	σ^2	168.20	158.57	163.97	165.69
M5	$V(6)$	12.22	12.45	12.46	12.60
	λ	1.228	1.224	1.224	1.221
	σ^2	457.28	446.27	446.52	440.82
	$V(7)$	18.38	18.68	18.77	19.02
M6	$V(6)$	12.72	13.82	14.06	14.14
	λ	1.097	1.099	1.099	1.102
	σ^2	248.32	252.96	252.42	258.17
	$V(5)$	7.37	7.51	7.52	7.58
M7	$V(6)$	14.40	14.91	14.90	15.00
	λ	1.066	1.065	1.069	1.072
	σ^2	185.58	181.77	188.38	191.63
	$V(7)$	18.00	18.37	18.52	18.62

Note: Polyhedral volumes and distortions were calculated using the computer program VOLCAL, written by L. W. Finger. The distortion parameters of mean quadratic elongation and angle variance are defined by Robinson et al. (1971).

TABLE 7. Linear thermal expansion and bulk compression coefficients for cell edges in pyroxmangite

A. α of cell edges ($\alpha = 1/\ell(\Delta\ell/\Delta T)$; T = 24 to 800 °C

$\alpha_a = 7.6 \times 10^{-6}$ °C^{-1}

$\alpha_b = 13.8 \times 10^{-6}$ °C^{-1}

$\alpha_c = 6.7 \times 10^{-6}$ °C^{-1}

B. β of cell edges ($\beta = 1/\ell(\Delta\ell/\Delta P)$; P = 1 bar to 20 kbar

$\beta_a = -2.9 \times 10^{-7}$ bar^{-1}

$\beta_b = -3.9 \times 10^{-7}$ bar^{-1}

$\beta_c = -3.8 \times 10^{-7}$ bar^{-1}

Controls on pyroxmangite-rhodonite phase equilibria

In a calorimetric study of synthetic pyroxmangite and rhodonite of $MnSiO_3$ composition, Navrotsky and Coons (1976) demonstrated that the two structures are remarkably alike in their thermodynamic properties, suggesting that the effects of surface energies, coherent intergrowths, and possible stacking defects would significantly affect the observed equilibria between these minerals. They further predicted that the close similarity between pyroxene and pyroxenoid structures could verge on continuous gradation between idealized end-member structures through incorporation of such lattice defects.

Throughout the high-temperature data collection described herein, the Ajiro pyroxmangite retained its structure even though by 800 °C it was almost undoubtedly well within the rhodonite stability field. During data collection, however, we noticed on the chart recorder the appearance of a small amount of peak splitting at temperatures of 400 °C and above. This splitting could be explained by incipient growth of rhodonite along the (001) plane, which is the plane shared by the W and P modules and is essentially identical in pyroxmangite and rhodonite. On comparing the data from all temperatures, a small amount of peak splitting was observed also at 24 °C, which, given the above interpretation, would indicate that there were small regions of rhodonite (one less P module) in the material at room temperature as well, although no conclusive evidence of streaking was observed on the 24 °C precession photographs.

Aikawa (1979, 1984) studied the orientation relationship of finely intergrown fibers of pyroxmangite and rhodonite caused by the experimental thermal transformation (at 1080 and 1100 °C) of pyroxmangite to rhodonite and determined that the crystal morphology is preserved

TABLE 6. Ajiro pyroxmangite cell parameters

	20 kbar	24 °C	200 °C	300 °C	400 °C	500 °C	600 °C	700 °C	800 °C
a (Å)	9.655(4)	9.712(2)	9.715(10)	9.719(9)	9.739(5)	9.740(8)	0.754(7)	0.760(6)	9.769(6)
b (Å)	10.453(4)	10.536(2)	10.549(6)	10.561(5)	10.585(4)	10.586(5)	10.617(6)	10.630(5)	10.649(6)
c (Å)	17.304(9)	17.438(3)	17.424(21)	17.448(22)	17.482(18)	17.481(21)	17.506(20)	17.525(16)	17.529(20)
α (°)	112.20(3)	112.15(1)	112.05(6)	112.08(6)	112.02(5)	111.97(6)	111.99(6)	111.93(5)	111.91(5)
β (°)	103.10(4)	102.88(1)	102.83(9)	102.78(9)	102.66(7)	102.63(9)	102.56(9)	102.54(7)	102.43(8)
γ (°)	82.92(3)	82.95(2)	82.94(6)	82.93(5)	82.97(4)	82.98(5)	82.97(5)	82.99(5)	83.02(5)
V_{cell} (Å^3)	1573.4(11)	1609.8(5)	1612.2(26)	1616.9(24)	1628.4(18)	1629.4(23)	1639.0(23)	1644.7(19)	1650.4(22)

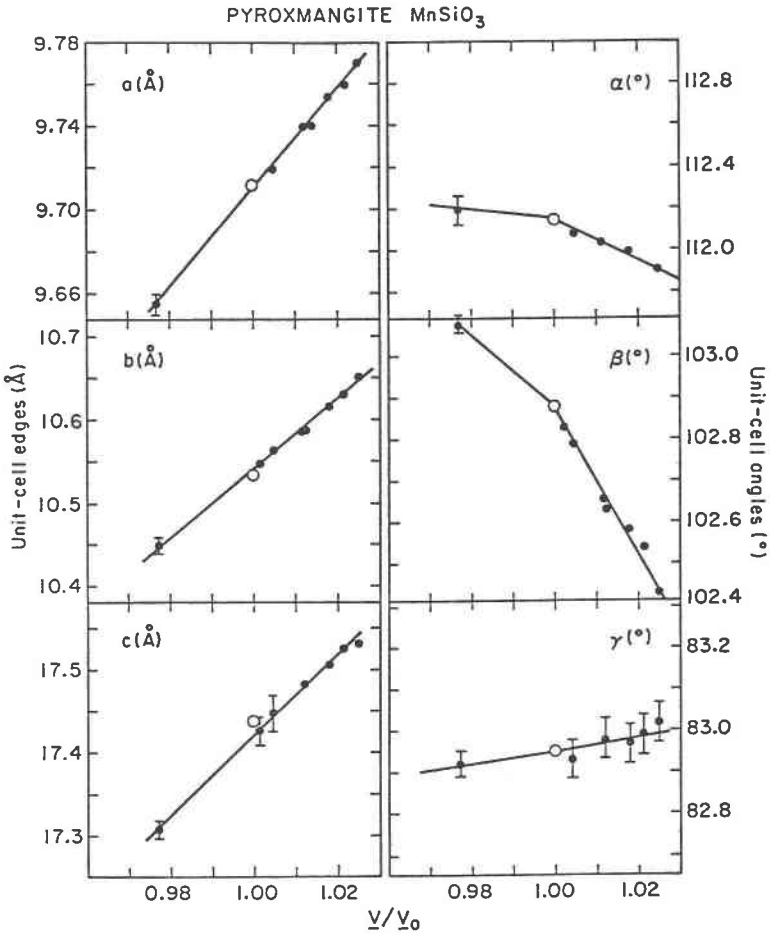

Fig. 1. Pyroxmangite unit-cell parameters versus V/V_0. High-temperature and high-pressure data are included.

and that c_p^* is parallel to c_r^*, which means that the (001) plane is shared by the two phases. The nature of the orientation is identical to that observed in natural intergrowths of the two minerals.

Recent studies of these minerals employing high-resolution transmission electron microscopy (HRTEM) by Alario Franco et al. (1980), Ried and Korekawa (1980), Czank and Liebau (1980), Veblen (1982, 1985), and Ried (1984) show that the phenomenon of coherent intergrowths in this system is widespread. In addition to conventional stacking faults along [100], which are common in wollastonite (e.g., Wenk, 1969) and have been noted in pyroxmangite as twinning (Diehl and Berdesinski, 1970) and as streaking along a^* (Chao et al., 1970), the HRTEM studies have shown that faults parallel to (001) are also common in pyroxenoids. These chain-periodicity faults (CPFs) consist of strips of one pyroxenoid, often only one unit cell wide, which are occasionally inserted parallel to the

TABLE 8. Principal strain components of expansion and compression due to temperature and pressure

Principal linear thermal-expansion coefficients	Orientation angle (°) with +a	+b	+c
A. Principal thermal expansion coefficients; T = 24 to 800 °C			
ϵ_1 17(1) × 10^{-6} °C^{-1}	70(7)	45(10)	73(7)
ϵ_2 12(1) × 10^{-6} °C^{-1}	56(7)	130(11)	59(5)
ϵ_3 3(1) × 10^{-6} °C^{-1}	139(5)	108(3)	37(5)
Volume-expansion coefficient: 32.4(2) × 10^{-6} °C^{-1}			
Principal linear compression coefficients	**Orientation angle (°) with +a**	**+b**	**+c**
B. Principal bulk compression coefficients; P = 1 bar to 20 kbar			
ϵ_1 −4.9(3) × 10^{-7} bar^{-1}	65(5)	83(11)	45(7)
ϵ_2 −4.0(2) × 10^{-7} bar^{-1}	95(6)	12(7)	111(9)
ϵ_3 −2.5(2) × 10^{-7} bar^{-1}	25(5)	80(6)	128(5)
Volume-compression coefficient: −11.4(4) × 10^{-7} bar^{-1}			

Note: Estimated standard deviations (×10^{-6} or 10^{-7} as appropriate) are given in parentheses.

TABLE 9. Tetrahedral chain angles in pryoxmangite at several temperatures

Chain angle	24 °C	200 °C	400 °C	600 °C
OC1-2-3	148.137(8)	148.90(4)	150.21(3)	151.21(4)
OC2-3-4	165.110(4)	165.13(2)	166.44(1)	167.39(2)
OC3-4-5	177.388(1)	177.38(1)	177.24(1)	177.37(1)
OC4-5-6	167.736(3)	166.89(2)	168.53(1)	168.56(1)
OC5-6-7	144.951(9)	144.17(4)	145.98(4)	145.96(4)
OC6-7-1	161.422(5)	161.38(3)	160.95(2)	160.94(3)
OC7-1-2	157.771(6)	156.82(3)	156.59(3)	156.14(3)

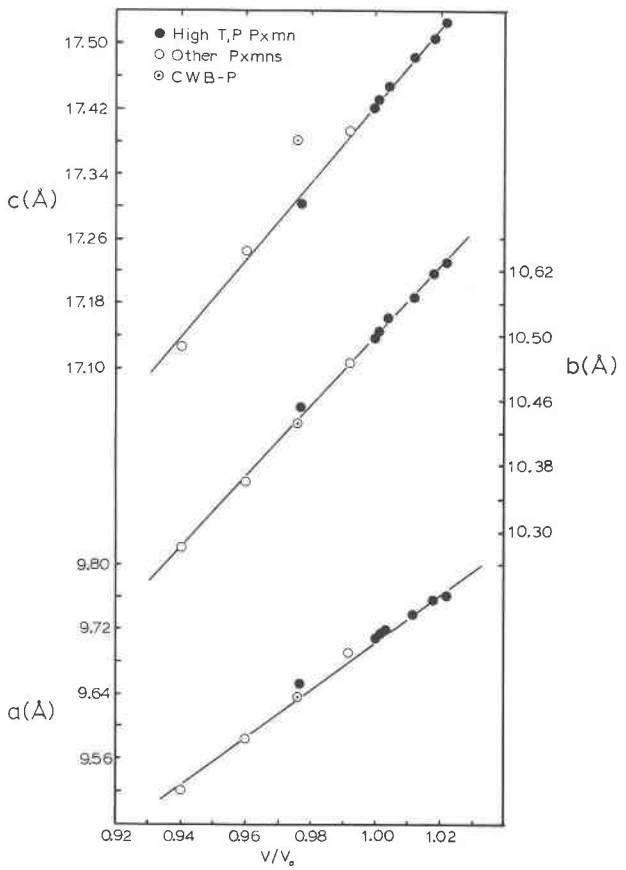

Fig. 2. Pyroxmangite unit-cell edges versus V/V_0. This plot includes pyroxmangites of other compositions (listed in Pinckney and Burnham, 1988) as well as the data from Fig. 1. The symbol CWB-P represents the Ca-rich pyroxferroite described by Burnham (1971). The slopes of the lines have been determined by a linear least-squares regression analysis of the data, excluding the pyroxferroite data for the *c*-axis plot.

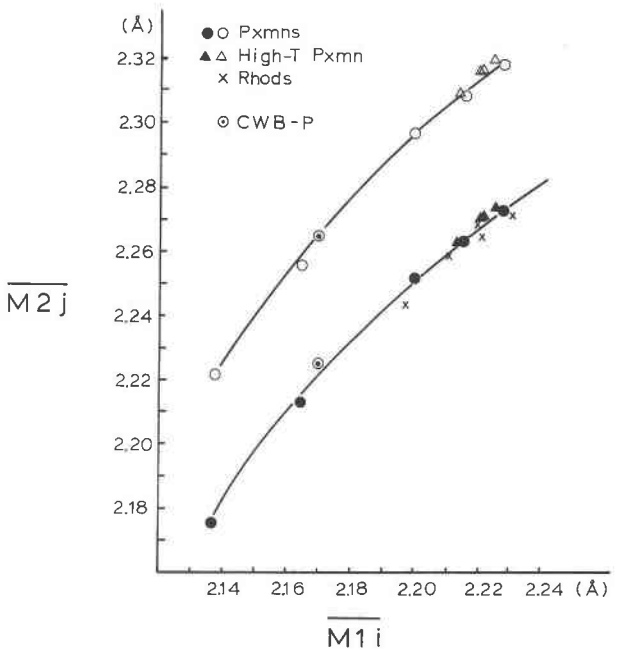

Fig. 3. Variation of $\overline{M2j}$ with $\overline{M1i}$ for all pyroxmangites and rhodonites considered in this and a separate study (Pinckney and Burnham, 1988). (The term $\overline{M1i}$ represents the grand mean M1*i*–O bond length, where the M1*i* octahedra comprise M1 through M3 in pyroxmangite and M1 and M2 in rhodonite. Similarly, $\overline{M2j}$ represents the grand mean M2*j*–O bond length.) The lower curve considers all M sites of pyroxmangite as six-coordinated except for M6 of CWB-P pyroxferroite, which is taken as five-coordinated. The upper curve considers M5 and M7 as seven-coordinated.

(001) plane into the parent matrix of a different pyroxenoid structure. Insertion of a pyroxmangite strip into rhodonite, for example, is equivalent to adding one pyroxene-layer module along (001). Unlike conventional stacking faults, which extend only partway across the crystal and result in considerable strain contrast across the fault, these CPFs extend completely across the crystal and produce no evident strain at the coherent boundary.

Czank and Liebau (1980) noted that the most common CPFs observed in the HRTEM studies are those involving one more or one less pyroxene module, particularly one more; that is, if the periodicity of the host phase is *n,* the most common CPF periodicity is $n + 2$. CPF periodicities of nine tetrahedra or greater are also commonly observed. Moreover, in experimental studies of this system, it has been noted that pyroxenoids with longer periodicities tend to crystallize metastably before transforming to the stable pyroxenoid phase (e.g., Momoi, 1974; Abrecht and Peter, 1980). These observations, as well as structural considerations discussed by Pinckney and Burnham (1988) suggest that the interfacial strain energy between two P modules, or PP, is less than that of WP, and that the strain energy for WW must be relatively high, as such a combination is never seen as a CPF. From this and from all of our observations thus far, we may conclude that the higher the chain periodicity *n,* the smaller the differences—structural, chemical, and thermodynamic—between the structures with periodicities *n* and $n + 2$ and the more likely that CPFs will be formed.

Given the widespread occurrence of such intergrowths,

TABLE 10. Mean thermal-expansion coefficients for mean M–O distances and polyhedral volumes: 24 to 600 °C

	$\alpha_{\overline{M-O}}$	α_V*
M1	0.601×10^{-5} °C^{-1}	5.69×10^{-5} °C^{-1}
M2	0.634×10^{-5} °C^{-1}	5.72×10^{-5} °C^{-1}
M3	1.107×10^{-5} °C^{-1}	7.14×10^{-5} °C^{-1}
M4	1.294×10^{-5} °C^{-1}	7.27×10^{-5} °C^{-1}
M5 (7)	0.543×10^{-5} °C^{-1}	5.68×10^{-5} °C^{-1}
(6)	0.173×10^{-5} °C^{-1}	5.41×10^{-5} °C^{-1}
M6 (6)	0.972×10^{-5} °C^{-1}	5.69×10^{-5} °C^{-1}
(5)	0.557×10^{-5} °C^{-1}	4.46×10^{-5} °C^{-1}
M7 (7)	0.252×10^{-5} °C^{-1}	5.70×10^{-5} °C^{-1}
(6)	1.184×10^{-5} °C^{-1}	6.28×10^{-5} °C^{-1}

* The mean thermal-expansion coefficients $\alpha_{\overline{M-O}}$ and α_V are computed from the equations $\alpha_{\overline{M-O}} = (1/(\overline{M-O})_{24\,°C}) \cdot \Delta(\overline{M-O})/\Delta T$ and $\alpha_V = (1/V_{24\,°C}) \cdot \Delta V/\Delta T$, where the slope of a linear regression equation applied to the data is used for the terms $\Delta(\overline{M-O})/\Delta T$ and $\Delta V/\Delta T$.

not only of the (001) chain-periodicity faults, but also of the (100) stacking faults and (010) chain-multiplicity faults seen in pyroxenes, pyroxenoids, and biopyriboles, the implications for mineralogy and petrology are profound. Since pyroxenes are used extensively as geothermometers and geobarometers to interpret geologic histories, it is important to realize that their coherent intergrowths with other biopyriboles and pyroxenoids could have significant effects on their thermochemical properties and hence on their utility as petrologic indicators. It is likely that metastable intergrowths are much more common in the pyroxenoid-pyroxene system than is currently believed, and, in fact, quite possible that structurally pure phases occur only rarely in this system.

Acknowledgments

We are grateful to Larry W. Finger and Robert M. Hazen for their invaluable advice and assistance with the high-temperature and high-pressure single-crystal experiments and to the Geophysical Laboratory of the Carnegie Institution of Washington, which generously provided one of us (L.R.P.) the facilities to carry out these experiments. Financial support for this research was provided by National Science Foundation grants EAR7622689 and EAR7920095 to C. W. Burnham.

References cited

Abrecht, J., and Peters, T. (1980) The miscibility gap between rhodonite and bustamite along the join $MnSiO_3$-$Ca_{0.60}Mn_{0.40}SiO_3$. Contributions to Mineralogy and Petrology, 74, 261–270.

Aikawa, N. (1979) Oriented intergrowth of rhodonite and pyroxmangite and their transformation mechanism. Mineralogical Journal of Japan, 9, 255–269.

——— (1984) Lamellar structure of rhodonite and pyroxmangite intergrowths. American Mineralogist, 69, 270–276.

Akimoto, S., and Syono, Y. (1972) High pressure transformations in $MnSiO_3$. American Mineralogist, 57, 76–84.

Alario Franco, M.A., Jefferson, D.A., Pugh, N.J., Thomas, J.M., and Bishop, A.C. (1980) Lattice imaging of structural defects in a chain silicate: The pyroxenoid mineral rhodonite. Materials Research Bulletin, 15, 73–79.

Burnham, C.W. (1971) The crystal structure of pyroxferroite from Mare Tranquillitatis. Proceedings of the Second Lunar Science Conference, 1, 47–57.

Burnham, C.W., Ohashi, Y., Hafner, S., and Virgo, D. (1971) Cation distribution and atomic thermal vibrations in an iron-rich orthopyroxene. American Mineralogist, 56, 850–876.

Busing, W.R., and Levy, H.A. (1964) The effect of thermal motion on the estimation of bond lengths from diffraction measurements. Acta Crystallographica, 17, 142–146.

Chao, E.C.T., Minkin, J.A., Frondel, C., Klein, C., Jr., Drake, J.C., Fuchs, L., Tani, B., Smith, J.V., Anderson, A.T., Moore, P.B., Zechman, J.R., Jr., Trail, R.J., Plant, A.G., Douglas, J.A.V., and Dence, M.R. (1970) Pyroxferroite, a new calcium-bearing silicate from Tranquillity Base. Proceedings of the Apollo 11 Lunar Science Conference, 1, 65–79.

Cromer, D.T. (1965) Anomalous dispersion corrections computed from self-consistent field relativistic Dirac-Slater wave functions. Acta Crystallographica, 18, 17–23.

Cromer, D.T., and Mann, J.B. (1968) X-ray scattering factors computed from numerical Hartree-Fock wave functions. Acta Crystallographica, A24, 321–324.

Czank, M., and Liebau, F. (1980) Periodicity faults in chain silicates: A new type of planar lattice fault observed with high resolution electron microscopy. Physics and Chemistry of Minerals, 6, 85–94.

Dent Glasser, L.S., and Glasser, F.P. (1961) Silicate transformations: Rhodonite-wollastonite. Acta Crystallographica, 14, 818–822.

Diehl, R., and Berdesinski, W. (1970) Zwillingsstellungen am Pyroxmangit der North Mine von Broken Hill, New South Wales, Australien. Neues Jahrbuch für Mineralogie Monatshefte, 348–362.

Finger, L.W., and Ohashi, Y. (1976) The thermal expansion of diopside to 800°C and a refinement of the crystal structure at 700°C. American Mineralogist, 61, 303–310.

Finger, L.W., and Prince, E. (1975) A system of FORTRAN IV computer programs for crystal structure computations. National Bureau of Standards (U.S.) Technical Note 854.

Finger, L.W., Hadidiacos, C., and Ohashi, Y. (1973) A computer-automated, single-crystal X-ray diffractometer. Carnegie Institution of Washington Year Book 72, 694–699.

Hazen, R.M., and Finger, L.W. (1977) Modifications in high-pressure, single-crystal diamond cell techniques. Carnegie Institution of Washington Year Book 76, 655–656.

Hazen, R.M., and Prewitt, C.T. (1977) Effects of temperature and pressure on interatomic distances in oxygen-based minerals. American Mineralogist, 62, 309–315.

Hazen, R.M., and Wones, D.R. (1978) Predicted and observed limits of trioctahedral micas. American Mineralogist, 63, 885–892.

Levien, L., and Prewitt, C.T. (1981) High-pressure study of diopside. American Mineralogist, 66, 315–323.

Maresch, W.V., and Mottana, A. (1976) The pyroxmangite-rhodonite transformation for the $MnSiO_3$ composition. Contributions to Mineralogy and Petrology, 55, 69–79.

Merrill, L., and Bassett, W.A. (1974) Miniature diamond anvil pressure cell for X-ray diffraction studies. Reviews of Scientific Instruments, 45, 290–294.

Momoi, H. (1974) Hydrothermal crystallization of $MnSiO_3$ polymorphs. Mineralogical Journal of Japan, 7, 359–373.

Morimoto, N., Koto, K., and Shinohara, T. (1966) Oriented transformation, johannsenite to bustamite. Mineralogical Journal of Japan, 5, 44–64.

Narita, H., Koto, K., and Morimoto, N. (1977) The crystal structures of $MnSiO_3$ polymorphs (rhodonite- and pyroxmangite-type). Mineralogical Journal of Japan, 8, 329–342.

Navrotsky, A., and Coons, W.E. (1976) Thermochemistry of some pyroxenes and related compounds. Geochimica et Cosmochimica Acta, 40, 1281–1288.

Ohashi, Y., and Burnham, C.W. (1973) Clinopyroxene lattice deformations: The roles of chemical substitution and temperature. American Mineralogist, 58, 843–849.

Ohashi, Y., and Finger, L.W. (1975) Pyroxenoids: A comparison of refined structures of rhodonite and pyroxmangite. Carnegie Institution of Washington Year Book 74, 564–569.

Pinckney, L.R., and Burnham, C.W. (1981) Possible diopside-bustamite transformation (abs.). EOS, 62, 417.

——— (1988) Effects of compositional variation on the crystal structures of pyroxmangite and rhodonite. American Mineralogist, 73, 798–808.

Pinckney, L.R., Finger, L.W., Hazen, R.M., and Burnham, C.W. (1981) Crystal structure of pyroxmangite at high temperature. Carnegie Institution of Washington Year Book 80, 380–384.

Ried, H. (1984) Intergrowth of pyroxene and pyroxenoid; chain periodicity faults in pyroxene. Physics and Chemistry of Minerals, 10, 230–235.

Ried, H., and Korekawa, M. (1980) Transmission electron microscopy of synthetic and natural Funferketten and Siebenerketten pyroxenoids. Physics and Chemistry of Minerals, 5, 351–365.

Robinson, K., Gibbs, G.V., and Ribbe, P.H. (1971) Quadratic elongation: A quantitative measure of distortion in coordination polyhedra. Science, 172, 567–570.

Rutstein, M.S. (1971) Re-examination of the wollastonite-hedenbergite ($CaSiO_3$-$CaFeSi_2O_6$) equilibria. American Mineralogist, 56, 2040–2052.

Veblen, D.R. (1982) Replacement of johannsenite by Mn-pyroxenoids: Microstructures and mechanisms of reaction. Geological Society of America Abstracts with Programs, 14, 637.

——— (1985) TEM study of a pyroxene-to-pyroxenoid reaction. American Mineralogist, 70, 885–901.

Wenk, H.-R. (1969) Polymorphism of wollastonite. Contributions to Mineralogy and Petrology, 22, 238–247.

Manuscript received July 15, 1986
Manuscript accepted March 4, 1988